

# Buckling and vibration analysis of laminated composite plate/shell structures via a smoothed quadrilateral flat shell element with in-plane rotations

H. Nguyen-Van<sup>a,c</sup>, N. Mai-Duy<sup>a</sup>, W. Karunasena<sup>b</sup>, T. Tran-Cong<sup>\*,a</sup>

<sup>a</sup>*Computational Engineering & Science Research Centre (CESRC), Faculty of Engineering and Surveying, University of Southern Queensland, QLD 4350, Australia*

<sup>b</sup>*Centre of Excellence in Engineered Fibre Composites (CEEFC), Faculty of Engineering and Surveying, University of Southern Queensland, QLD 4350, Australia*

<sup>c</sup>*Current address: Faculty of Civil Engineering, HoChiMinh City University of Architecture, 196 Pasteur, District 3, HCM 70000, Vietnam*

---

## Abstract

This paper presents buckling and free vibration analysis of composite plate/shell structures of various shapes, modulus ratios, span-to-thickness ratios, boundary conditions and lay-up sequences via a novel smoothed quadrilateral flat element. The element is developed by incorporating a strain smoothing technique into a flat shell approach. As a result, the evaluation of membrane, bending and geometric stiffness matrices are based on integration along the boundary of smoothing elements, which leads to accurate numerical solutions even with badly-shaped elements. Numerical examples and comparison with other existing solutions show that the present element is efficient, accurate and free of locking.

*Key words:* buckling response, natural vibration, laminated composite plate and shell, strain smoothing method, locking-free.

---

## 1. Introduction

The extensive use of laminated composites in various types of plates and shells is of considerable interests to many researchers in the field of modelling, analysis and design of these structures. Accurate prediction of structural response characteristics is a challenging problem for the analysis of laminated composites due to the anisotropic structural behaviour and the presence of various types of complicated constituent couplings. Buckling and vibration response of plate and shell are one of

---

\*Correspondence author: Tel. +61 7 46312539, Fax. +61 7 46312526.  
*Email address:* trancong@usq.edu.au (T. Tran-Cong)

many important considerations of engineering design and a thorough study of stability behaviours and natural vibrations of these structures is essential in assessing their full potential.

Numerical methods such as finite element methods have been developed and widely used for the analysis of buckling and natural vibration responses of laminated composite plates/shells. The body of works is too large to list altogether here. An excellent review of the development of plate/shell finite elements during the past 20 years was presented by Yang et al [1]. More details and reviews of the literature on laminated composite plates/shells may be found in Leissa [2] and Aydogu [3] for buckling analysis and in Mohamad [4] and Liew's group [5, 6, 7, 8, 9] for vibration analysis.

As discussed in many references [10, 11, 12, 13, 14, 15], flat elements have been often and widely used owing to the ease to mix these with other types of element, the simplicity in their formulation and the effectiveness in performing computation. In addition, the inclusion of transverse shear effect with the aid of Reissner-Mindlin kinematics and the incorporation of drilling degrees of freedom significantly improved the performance of the flat elements for moderately thick to thin plate/shell structures [15].

The objective of the present study is to further develop the flat element MISQ24, whose performance in geometrically linear static analysis and the effect of smoothing have already been verified and demonstrated in reference [16], for buckling and natural vibration analysis of composite plate and shell structures. In this study, the consistent mass matrix is used in the dynamic formulation while the strain smoothing operator is incorporated in the formulation of the geometric stiffness matrix for buckling analysis. Stability and free vibration analysis of various composite plates/shells are performed in order to have a better understanding of their behaviours associated with all relevant parameters such as boundary conditions (simply supported, clamped, free and mixed combinations), types of laminates (symmetric/asymmetric cross-ply, angle-ply), number of layers, mesh distortion, fibre orientations, span-to-thickness ratios and modulus ratios. Comparison of the numerical results obtained using the MISQ24 element with analytic solutions and other FSDT-based, HSDT-based elements also forms a major part of the present investigation.

In the following sections, a brief review of the FSDT-based finite element formu-

lation of four-node flat shell element with drilling DOFs is first introduced. This is followed by the strain smoothing approach for the flat shell finite element. Numerical examples are then employed to investigate and assess the performance of the proposed flat shell element in buckling and free vibration analyses, followed by some conclusions.

## 2. A flat shell element formulation based on the first-order shear deformation theory

### 2.1. Governing equations

In the first-order shear deformation theory (FSDT) [17], the flat shell kinematics is governed by the midsurface displacement  $u_0, v_0, w_0$  and rotation  $\theta_x, \theta_y$  as follows.

$$\begin{aligned} u(x, y, z) &= u_0(x, y) + z\theta_x, \\ v(x, y, z) &= v_0(x, y) + z\theta_y, \\ w(x, y, z) &= w_0(x, y). \end{aligned} \quad (1)$$

where  $(u_0, v_0, w_0)$  are the displacements of a point situated in the middle surface (an  $xy$  surface), and  $\theta_x, \theta_y$  are the rotations of the transverse normal, i.e. in the  $z$  direction, about the  $y$ - and  $x$ - axes, respectively (see Figure 1).

The in-plane strain vector  $\boldsymbol{\epsilon} = [\varepsilon_x \quad \varepsilon_y \quad \varepsilon_{xy}]^T$  can be written as

$$\boldsymbol{\epsilon} = \begin{bmatrix} u_{o,x} \\ v_{o,y} \\ u_{o,y} + v_{o,x} \end{bmatrix} + z \begin{bmatrix} \theta_{x,x} \\ \theta_{y,y} \\ \theta_{x,y} + \theta_{y,x} \end{bmatrix} = \boldsymbol{\epsilon}_m + z\boldsymbol{\epsilon}_b, \quad (2)$$

and the transverse shear strain vector as

$$\boldsymbol{\gamma} = [\gamma_{xz} \quad \gamma_{yz}]^T = [\theta_x - w_{,x} \quad \theta_y - w_{,y}]^T. \quad (3)$$

For an anisotropic laminated shell, the stress resultant constitutive relationships are expressed as follows.

$$\boldsymbol{\sigma}_p = \begin{Bmatrix} \mathbf{N} \\ \mathbf{M} \end{Bmatrix} = \begin{bmatrix} \mathbf{A} & \mathbf{B} \\ \mathbf{B} & \mathbf{D} \end{bmatrix} \begin{Bmatrix} \boldsymbol{\epsilon}_m \\ \boldsymbol{\epsilon}_b \end{Bmatrix} = \mathbf{C}_p \boldsymbol{\epsilon}_p, \quad (4)$$

$$\mathbf{T} = \begin{bmatrix} k_1^2 \bar{C}_{55}^0 & k_1 k_2 \bar{C}_{45}^0 \\ k_1 k_2 \bar{C}_{45}^0 & k_2^2 \bar{C}_{44}^0 \end{bmatrix} \begin{Bmatrix} \gamma_{xz} \\ \gamma_{yz} \end{Bmatrix} = \mathbf{C}_s \boldsymbol{\gamma}, \quad (5)$$

where  $\mathbf{N} = [N_x \quad N_y \quad N_{xy}]^T$ ,  $\mathbf{M} = [M_x \quad M_y \quad M_{xy}]^T$ ,  $\mathbf{T} = [Q_x \quad Q_y]^T$  are the membrane force vector, the bending moment vector and the transverse shear force vector,

respectively;  $k_1^2, k_2^2$  are shear correction factors (SCFs) which can be estimated by using special methods [18];  $\mathbf{A}, \mathbf{B}, \mathbf{D}, \mathbf{C}_s$  are matrices of extensional stiffness, bending-extensional coupling stiffness, bending stiffness and transverse shearing stiffness, respectively defined as

$$\begin{aligned} (A_{ij}, B_{ij}, D_{ij}) &= \int_{-h/2}^{h/2} (1, z, z^2) \bar{Q}_{ij} dz, & i, j &= 1, 2, 6 \\ C_{ij}^0 &= \int_{-h/2}^{h/2} \bar{Q}_{ij} dz, & i, j &= 4, 5 \end{aligned} \quad (6)$$

where  $h$  is the thickness of the plate,  $\bar{Q}_{ij}$  are the elastic constants with respect to the global  $x$ -axis and their detailed definitions can be found in Reference [17].

## 2.2. Finite element formulation of the 4-node flat shell element with in-plane rotations

### 2.2.1. Membrane part

The 4-node membrane element with drilling DOFs (Figure 2) is derived by combining the in-plane displacements using Allman-type interpolation functions [19] and the standard bilinear independent normal (drilling) rotation fields. Details of the formulation can be found in the original reference [20] and only a brief review is presented here.

The independent rotation field is interpolated according to

$$\theta_z = \sum_{i=1}^4 N_i(\xi, \eta) \theta_{zi}, \quad (7)$$

and the in-plane displacement fields are approximated by the Allman-type interpolation

$$\mathbf{u} = \begin{bmatrix} u \\ v \end{bmatrix} = \sum_{i=1}^4 N_i(\xi, \eta) \begin{bmatrix} u_i \\ v_i \end{bmatrix} + \frac{1}{8} \sum_{k=5}^8 N_k(\xi, \eta) (\theta_{zj} - \theta_{zi}) \begin{bmatrix} y_{ij} \\ x_{ij} \end{bmatrix}, \quad (8)$$

where

$$x_{ij} = x_j - x_i, \quad y_{ij} = y_j - y_i, \quad (9)$$

$$N_i(\xi, \eta) = \frac{1}{4} (1 + \xi_i \xi) (1 + \eta_i \eta) \quad i = 1, 2, 3, 4 \quad (10)$$

$$N_k(\xi, \eta) = \frac{1}{2} (1 - \xi^2) (1 + \eta_k \eta) \quad k = 5, 7 \quad (11)$$

$$N_k(\xi, \eta) = \frac{1}{2} (1 + \xi_k \xi) (1 - \eta^2) \quad k = 6, 8. \quad (12)$$

and the ordered triplets  $(k, i, j)$  are given by (5, 1, 2), (6, 2, 3), (7, 3, 4), (8, 4, 1)

The linear strain matrix is given by

$$\boldsymbol{\epsilon}_m = \text{symm} \nabla \mathbf{u} = \sum_{i=1}^4 \mathbf{B}_{mi} \mathbf{u}_i, \quad (13)$$

where  $\mathbf{u}_i = [u_i \quad v_i \quad \theta_{zi}]^T$  is the nodal displacement vector and the gradient matrix  $\mathbf{B}_{mi}$  has the following form

$$\mathbf{B}_{mi} = \begin{bmatrix} N_{i,x} & 0 & Nx_{i,x} \\ 0 & N_{i,y} & Ny_{i,y} \\ N_{i,y} & N_{i,x} & Nx_{i,y} + Ny_{i,x} \end{bmatrix}, \quad (14)$$

in which  $Nx$ ,  $Ny$  are Allman's incompatible shape functions defined as

$$Nx_i = \frac{1}{8}(y_{ij}N_l - y_{ik}N_m), \quad (15)$$

$$Ny_i = \frac{1}{8}(x_{ij}N_l - x_{ik}N_m). \quad (16)$$

Furthermore, the skew-symmetric part of the strain tensor ( $\boldsymbol{\epsilon}_{sk}$ ) can be expressed as

$$\boldsymbol{\epsilon}_{sk} = \text{skew} \nabla \mathbf{u} = \sum_{i=1}^4 \mathbf{b}_i \mathbf{u}_i + \theta_z, \quad (17)$$

where

$$\mathbf{b}_i = \begin{bmatrix} -\frac{1}{2}N_{i,y} \\ \frac{1}{2}N_{i,x} \\ \frac{1}{16}(-y_{ij}N_{l,y} + y_{ik}N_{m,y} + x_{ij}N_{l,x} - x_{ik}N_{m,x}) - N_i \end{bmatrix}, \quad (18)$$

The variational formulation suggested by [21] is described as

$$\Pi_\gamma(\mathbf{u}, \theta_z) = \frac{1}{2} \int_\Omega \boldsymbol{\epsilon}_m^T \mathbf{D}_m \boldsymbol{\epsilon}_m d\Omega + \frac{1}{2} \gamma \int_\Omega (\boldsymbol{\epsilon}_{sk} - \theta_z)^2 d\Omega - \int_\Omega \mathbf{u}^T \mathbf{f} d\Omega. \quad (19)$$

Minimization of Equation (19) results in the element membrane stiffness matrix  $\mathbf{K}_{mem}$ , which is the sum of matrix  $\mathbf{K}_m$  and a penalty matrix  $\mathbf{P}_\gamma$  as follows.

$$\mathbf{K}_{mem} = \mathbf{K}_m + \mathbf{P}_\gamma = \int_\Omega \mathbf{B}_m^T \mathbf{D}_m \mathbf{B}_m d\Omega + \gamma \int_\Omega \mathbf{b}^T \mathbf{b} d\Omega. \quad (20)$$

where  $\mathbf{D}_m = \mathbf{A}$  is material rigidity matrix for membrane.

The positive penalty parameter  $\gamma$  in Equation (20) is problem dependent. For isotropic elasticity, the formulation is reported to be insensitive to the value of  $\gamma$  which is taken as the shear modulus value ( $\gamma = G$ ) [20]. However, many recent numerical studies showed that the smaller value of  $\gamma$  (i.e. value of  $\gamma/G$  between 1/10000 and 1) appeared to give more accurate solutions [22, 23, 13]. In this study,  $\gamma/G_{12} = 1/1000$  is used for composite material.

### 2.2.2. Plate-bending part

For the plate bending component of the flat shell element, the Mindlin-Reissner type 4-node plate element is employed (Figure 3).

The displacement field  $\mathbf{u}$  is approximated as

$$\mathbf{u} = [w \quad \theta_x \quad \theta_y]^T = \sum_{i=1}^4 \mathbf{N}_i \mathbf{u}_i, \quad (21)$$

where  $\mathbf{N}_i$  is the bilinear shape function as in Equation (10) and  $\mathbf{u}_i = [w_i \quad \theta_{xi} \quad \theta_{yi}]$  is the nodal displacement vector of the element.

The corresponding approximation of curvature is given by

$$\kappa = \begin{bmatrix} \theta_{x,x} \\ \theta_{y,y} \\ \theta_{x,y} + \theta_{y,x} \end{bmatrix} = \mathbf{B}_b \mathbf{u}, \quad (22)$$

where

$$\mathbf{B}_{bi} = \begin{pmatrix} 0 & N_{i,x} & 0 \\ 0 & 0 & N_{i,y} \\ 0 & N_{i,y} & N_{i,x} \end{pmatrix}. \quad (23)$$

The shear strain is approximated with independent interpolation schemes in the natural coordinate system [24]

$$\begin{bmatrix} \gamma_x \\ \gamma_y \end{bmatrix} = \mathbf{J}^{-1} \begin{bmatrix} \gamma_\xi \\ \gamma_\eta \end{bmatrix} = \mathbf{J}^{-1} \begin{bmatrix} \frac{1}{2}(1-\xi) & 0 & \frac{1}{2}(1+\xi) & 0 \\ 0 & \frac{1}{2}(1-\eta) & 0 & \frac{1}{2}(1+\eta) \end{bmatrix} \begin{bmatrix} \gamma_\eta^A \\ \gamma_\xi^B \\ \gamma_\eta^C \\ \gamma_\xi^D \end{bmatrix}, \quad (24)$$

in which  $\mathbf{J}$  is the Jacobian matrix and the midside nodes A, B, C, D are shown in Figure 3. Expressing  $\gamma_\eta^A$ ,  $\gamma_\eta^C$  and  $\gamma_\xi^B, \gamma_\xi^D$  in terms of the discretized fields  $\mathbf{u}$ , we obtain the shear matrix

$$\bar{\mathbf{B}}_{si} = \mathbf{J}^{-1} \begin{bmatrix} N_{i,\xi} & b_i^{11} N_{i,\xi} & b_i^{12} N_{i,\xi} \\ N_{i,\eta} & b_i^{21} N_{i,\eta} & b_i^{22} N_{i,\eta} \end{bmatrix}, \quad (25)$$

where

$$b_i^{11} = \xi_i x_{,\xi}^M, \quad b_i^{12} = \xi_i y_{,\xi}^M, \quad b_i^{21} = \eta_i x_{,\eta}^L, \quad b_i^{22} = \eta_i y_{,\eta}^L, \quad (26)$$

in which  $\xi_i \in \{-1, 1, 1, -1\}$ ,  $\eta_i \in \{-1, -1, 1, 1\}$

and  $(i, M, L) \in \{(1, B, A); (2, B, C); (3, D, C); (4, D, A)\}$ .

Then through the direct application of variational principles, the element plate-bending stiffness matrix can be obtained as follows.

$$\mathbf{K}_p = \mathbf{K}_b + \mathbf{K}_s = \int_{\Omega^e} \mathbf{B}_b^T \mathbf{D}_b \mathbf{B}_b d\Omega + \int_{\Omega^e} \bar{\mathbf{B}}_s^T \mathbf{D}_s \bar{\mathbf{B}}_s d\Omega, \quad (27)$$

where  $\mathbf{D}_b = \mathbf{D}$ ,  $\mathbf{D}_s = \mathbf{C}_s$  are material rigidity matrices for bending and shear, respectively.

### 2.2.3. Construction of a flat shell element

The plate bending and membrane formulations presented in the above sections can be combined to form a four-node flat shell element. When all nodes of the flat shell element are placed in the mid-thickness surface of the shell, the stiffness matrix of a shell element can be formed as

$$\mathbf{K}_{flat} = \begin{bmatrix} \mathbf{K}_m + \mathbf{P}_\gamma & \mathbf{K}_{mb} \\ \mathbf{K}_{mb}^T & \mathbf{K}_p \end{bmatrix}, \quad (28)$$

where the membrane-bending coupling stiffness matrix  $\mathbf{K}_{mb}$  is given by

$$\mathbf{K}_{mb} = \int_{\Omega} \mathbf{B}_m \mathbf{B} \mathbf{B}_b d\Omega \quad (29)$$

For some shells with double curvature, it may not be possible to have all four nodes of the flat shell element on the same plane (warped geometries) and the flat element stiffness must be modified before transformation to the global reference system by using the rigid link correction suggested by Taylor [25]. For the rigid link correction, the mean plane is formed by connecting central points of each side and distances between the mean plane and each nodes are taken to be the same ( $|z_i| = h$ ). Then, the following displacement transformation equation at each node  $i$  is employed to transform the nodal variables to the projected flat element variables

$$\mathbf{q}'_i = \begin{Bmatrix} u'_i \\ v'_i \\ w'_i \\ \theta'_{xi} \\ \theta'_{yi} \\ \theta'_{zi} \end{Bmatrix} = \begin{bmatrix} 1 & 0 & 0 & 0 & 0 & 0 \\ 0 & 1 & 0 & 0 & 0 & 0 \\ 0 & 0 & 1 & 0 & 0 & 0 \\ 0 & z_i & 0 & 1 & 0 & 0 \\ -z_i & 0 & 0 & 0 & 1 & 0 \\ 0 & 0 & 0 & 0 & 0 & 1 \end{bmatrix} \begin{Bmatrix} u_i \\ v_i \\ w_i \\ \theta_{xi} \\ \theta_{yi} \\ \theta_{zi} \end{Bmatrix} = \mathbf{W}_i \mathbf{q}_i, \quad (30)$$

where  $\mathbf{W}$  is the projection matrix and  $z_i$  defines the warpage offset at each node  $i$  perpendicular to the flat mean plane as shown in Figure 4.

The local element stiffness matrix, considering the warping effects, is obtained as

$$\mathbf{K}_{local} = \mathbf{W} \mathbf{K}_{flat} \mathbf{W}^T. \quad (31)$$

The element stiffness in the global reference system  $\mathbf{K}_{global}$  is then obtained via the standard rotation matrix  $\mathbf{R}$  [26] as

$$\mathbf{K}_{global} = \mathbf{R}^T \mathbf{K}_{local} \mathbf{R}. \quad (32)$$

Through the direct application of variational principles, the eigenvalue equation for free vibration analysis is given as

$$(\mathbf{K} - \omega^2 \mathbf{M}) \mathbf{q} = 0, \quad (33)$$

where  $\omega$  is the natural frequency and  $\mathbf{M}$  is the global mass matrix which is defined by

$$\mathbf{M} = \int_{\Omega} \mathbf{N}^T \mathbf{m} \mathbf{N} d\Omega, \quad \mathbf{m} = \rho h \begin{bmatrix} 1 & 0 & 0 & 0 & 0 \\ 0 & 1 & 0 & 0 & 0 \\ 0 & 0 & 1 & 0 & 0 \\ 0 & 0 & 0 & \frac{h^2}{12} & 0 \\ 0 & 0 & 0 & 0 & \frac{h^2}{12} \end{bmatrix}, \quad (34)$$

and for buckling analysis

$$(\mathbf{K} - \lambda \mathbf{K}_g) \mathbf{q} = 0, \quad (35)$$

where  $\lambda$  is the critical buckling load and  $\mathbf{K}_g$  is the geometric stiffness matrix which is defined by

$$\mathbf{K}_g = \int_{\Omega} \mathbf{B}_g^T \hat{\boldsymbol{\sigma}}_0 \mathbf{B}_g d\Omega, \quad (36)$$

in which

$$\boldsymbol{\sigma}_0 = \begin{bmatrix} \sigma_x^0 & \sigma_{xy}^0 \\ \sigma_{xy}^0 & \sigma_y^0 \end{bmatrix}, \quad \hat{\boldsymbol{\sigma}}_0 = \begin{bmatrix} h\boldsymbol{\sigma}_0 & 0 & 0 \\ 0 & \frac{h^3}{12}\boldsymbol{\sigma}_0 & 0 \\ 0 & 0 & \frac{h^3}{12}\boldsymbol{\sigma}_0 \end{bmatrix}, \quad \mathbf{B}_{gi} = \begin{bmatrix} N_{i,x} & 0 & 0 \\ N_{i,y} & 0 & 0 \\ 0 & N_{i,x} & 0 \\ 0 & N_{i,y} & 0 \\ 0 & 0 & N_{i,x} \\ 0 & 0 & N_{i,y} \end{bmatrix}. \quad (37)$$

### 3. Strain smoothing approach for flat shell finite element

#### 3.1. Smoothed membrane strain approximation

The membrane strains at an arbitrary point  $\mathbf{x}_C$  can be obtained by using the following strain smoothing operation

$$\tilde{\boldsymbol{\epsilon}}_m(\mathbf{x}_C) = \int_{\Omega_C} \boldsymbol{\epsilon}_m(\mathbf{x}) \Phi(\mathbf{x} - \mathbf{x}_C) d\Omega, \quad (38)$$

where  $\epsilon_m$  is the membrane strain obtained from displacement compatibility condition as given in Equation (13);  $\Omega_C$  is the smoothing cell domain on which the smoothing operation is performed ( $\Omega_C$  may be an entire element or part of an element as shown in Figure 5);  $\Phi$  is a given smoothing function that satisfies at least unity property  $\int_{\Omega_C} \Phi d\Omega = 1$  and, in the present work, is defined as

$$\Phi(\mathbf{x} - \mathbf{x}_C) = \begin{cases} 1/A_C & \mathbf{x} \in \Omega_C, \\ 0 & \mathbf{x} \notin \Omega_C, \end{cases} \quad (39)$$

in which  $A_C = \int_{\Omega_C} d\Omega$  is the area of a smoothing cell (subcell).

Substituting  $\Phi$  into Equation (38) and applying the divergence theorem, one can get a smoothed membrane strain

$$\tilde{\epsilon}_m(\mathbf{x}_C) = \frac{1}{2A_C} \int_{\Omega_C} \left( \frac{\partial u_i}{\partial x_j} + \frac{\partial u_j}{\partial x_i} \right) d\Omega = \frac{1}{2A_C} \int_{\Gamma_C} (u_i n_j + u_j n_i) d\Gamma, \quad (40)$$

where  $\Gamma_C$  is the boundary of the smoothing cell.

Introducing the finite element approximation of  $\mathbf{u}_m = [u \ v \ \theta_z]^T$  into Equation (40) gives

$$\tilde{\epsilon}_m(\mathbf{x}_C) = \tilde{\mathbf{B}}_m(\mathbf{x}_C) \mathbf{u}_m, \quad (41)$$

where

$$\mathbf{u}_{mi} = [u_i \ v_i \ \theta_{zi}]^T, \quad (42)$$

$$\tilde{\mathbf{B}}_{mi}(\mathbf{x}_C) = \frac{1}{A_C} \int_{\Gamma_C} \begin{pmatrix} N_i n_x & 0 & N x_i n_x \\ 0 & N_i n_y & N y_i n_y \\ N_i n_y & N_i n_x & N x_i n_y + N y_i n_x \end{pmatrix} d\Gamma. \quad (43)$$

Applying Gauss integration along the four segments of the boundary  $\Gamma_C$  of the smoothing domain  $\Omega_C$ , the above equation can be rewritten in algebraic form as

$$\tilde{\mathbf{B}}_{mi}(\mathbf{x}_C) = \frac{1}{A_C} \sum_{b=1}^4 \begin{pmatrix} \sum_{n=1}^{nG} w_n N_i(\mathbf{x}_{bn}) n_x & 0 & 0 \\ 0 & \sum_{n=1}^{nG} w_n N_i(\mathbf{x}_{bn}) n_y & 0 \\ \sum_{n=1}^{nG} w_n N_i(\mathbf{x}_{bn}) n_y & \sum_{n=1}^{nG} w_n N_i(\mathbf{x}_{bn}) n_x & 0 \end{pmatrix} + \frac{1}{A_C} \sum_{b=1}^4 \begin{pmatrix} 0 & 0 & \sum_{n=1}^{nG} w_n N x_i(\mathbf{x}_{bn}) n_x \\ 0 & 0 & \sum_{n=1}^{nG} w_n N y_i(\mathbf{x}_{bn}) n_y \\ 0 & 0 & \sum_{n=1}^{nG} w_n N x_i(\mathbf{x}_{bn}) n_y + \sum_{n=1}^{nG} w_n N y_i(\mathbf{x}_{bn}) n_x \end{pmatrix} \quad (44)$$

where  $nG$  is the number of Gauss integration points,  $\mathbf{x}_{bn}$  the Gauss point and  $w_n$  the corresponding weighting coefficients. The first term in Equation (44), which involves only bilinear shape functions, is evaluated by one Gauss point ( $nG = 1$ ). The second term, involving quadratic shape functions, is computed using two Gauss points ( $nG = 2$ ).

The smoothed membrane element stiffness matrix can be obtained as

$$\begin{aligned}\tilde{\mathbf{K}}_{mem} &= \tilde{\mathbf{K}}_m + \mathbf{P}_\gamma = \int_{\Omega} \tilde{\mathbf{B}}_m^T \mathbf{D}_m \tilde{\mathbf{B}}_m d\Omega + \gamma \int_{\Omega} \mathbf{b}^T \mathbf{b} d\Omega \\ &= \sum_{C=1}^{nc} \tilde{\mathbf{B}}_{mC}^T \mathbf{D}_m \tilde{\mathbf{B}}_{mC} A_C + \gamma \int_{\Omega} \mathbf{b}^T \mathbf{b} d\Omega\end{aligned}\quad (45)$$

in which  $nc$  is the number of smoothing cells. In the present method  $nc = 1$  is used and the penalty matrix  $\mathbf{P}_\gamma$  is integrated using a 1-point Gauss quadrature to suppress a spurious, zero-energy mode associated with the drilling DOFs [20].

### 3.2. Smoothed plate-bending strain approximation

In a similar way, by using the same constant smoothing function  $\Phi$  as for membrane strain, the smoothed curvature matrix can be obtained as

$$\tilde{\kappa}(\mathbf{x}_C) = \int_{\Omega_C} \kappa(\mathbf{x}) \Phi(\mathbf{x} - \mathbf{x}_C) d\Omega = \frac{1}{2A_C} \int_{\Gamma_C} (\theta_i n_j + \theta_j n_i) d\Gamma. \quad (46)$$

Then the relationship between the smoothed curvature field and the nodal displacement is written as

$$\tilde{\kappa}(\mathbf{x}_C) = \tilde{\mathbf{B}}_b(\mathbf{x}_C) \mathbf{u}_b, \quad (47)$$

where

$$\mathbf{u}_{bi} = [w_i \ \theta_{xi} \ \theta_{yi}]^T, \quad (48)$$

$$\tilde{\mathbf{B}}_{bi}(\mathbf{x}_C) = \frac{1}{A_C} \int_{\Gamma_C} \begin{pmatrix} 0 & N_i n_x & 0 \\ 0 & 0 & N_i n_y \\ 0 & N_i n_y & N_i n_x \end{pmatrix} d\Gamma. \quad (49)$$

Using integration with one-point Gauss quadrature to evaluate the above equation over the four boundary segment of the smoothing cell we obtain

$$\tilde{\mathbf{B}}_{bi}(\mathbf{x}_C) = \frac{1}{A_C} \sum_{b=1}^4 \begin{pmatrix} 0 & N_i(\mathbf{x}_b^G) n_x & 0 \\ 0 & 0 & N_i(\mathbf{x}_b^G) n_y \\ 0 & N_i(\mathbf{x}_b^G) n_y & N_i(\mathbf{x}_b^G) n_x \end{pmatrix} l_{bC}. \quad (50)$$

Finally, the plate-bending element stiffness matrix in Equation (27) can be transformed as follows

$$\tilde{\mathbf{K}}_p = \tilde{\mathbf{K}}_b + \mathbf{K}_s = \sum_{C=1}^{nc} \tilde{\mathbf{B}}_b^T \mathbf{D}_b \tilde{\mathbf{B}}_b A_C + \int_{\Omega_e} \mathbf{B}_s^T \mathbf{D}_s \mathbf{B}_s d\Omega. \quad (51)$$

In Equation (51), the shear term  $\mathbf{K}_s$  is still computed by  $2 \times 2$  Gauss quadrature [24] while the element bending stiffness  $\tilde{\mathbf{K}}_b$  is computed by one Gaussian point along each segment of the smoothing cells of the element. In this study, two smoothing cells ( $nc = 2$ ) as shown in Figure 5 are used for calculating the smoothed bending stiffness matrix of the element.

The flat shell element stiffness matrix in Equation (28) is then rewritten as

$$\tilde{\mathbf{K}}_{flat} = \begin{bmatrix} \tilde{\mathbf{K}}_m + \mathbf{P}_\gamma & \tilde{\mathbf{K}}_{mb} \\ \tilde{\mathbf{K}}_{mb}^T & \tilde{\mathbf{K}}_p \end{bmatrix}, \quad (52)$$

where the smoothed membrane-bending coupling stiffness matrix  $\tilde{\mathbf{K}}_{mb}$  is given by

$$\tilde{\mathbf{K}}_{mb} = \int_{\Omega} \tilde{\mathbf{B}}_m^T \mathbf{B} \tilde{\mathbf{B}}_b d\Omega = \sum_{C=1}^1 \tilde{\mathbf{B}}_{mC}^T \mathbf{B} \tilde{\mathbf{B}}_{bC} A_C. \quad (53)$$

### 3.3. Smoothed geometric stiffness matrix

Similarly, the smoothed geometric strain over the element domain  $\Omega_C$  can be written as

$$\tilde{\boldsymbol{\epsilon}}_g(\mathbf{x}_C) = \tilde{\mathbf{B}}_g(\mathbf{x}_C) \mathbf{q}_b \quad (54)$$

where

$$\mathbf{q}_b = [w_i \quad \theta_{xi} \quad \theta_{yi}], \quad (55)$$

$$\tilde{\mathbf{B}}_{gi}(\mathbf{x}_C) = \frac{1}{A_C} \int_{\Gamma_C} \begin{pmatrix} N_i n_x & 0 & 0 \\ N_i n_y & 0 & 0 \\ 0 & N_i n_x & 0 \\ 0 & N_i n_y & 0 \\ 0 & 0 & N_i n_x \\ 0 & 0 & N_i n_y \end{pmatrix} d\Gamma \quad (56)$$

Equation (56) can be evaluated with one-point Gauss quadrature integration along the four boundary segments of the smoothing cell as follows

$$\tilde{\mathbf{B}}_{gi}(\mathbf{x}_C) = \frac{1}{A_C} \sum_{g=1}^4 \begin{pmatrix} N_i(\mathbf{x}_g^G) n_x & 0 & 0 \\ N_i(\mathbf{x}_g^G) n_y & 0 & 0 \\ 0 & N_i(\mathbf{x}_g^G) n_x & 0 \\ 0 & N_i(\mathbf{x}_g^G) n_y & 0 \\ 0 & 0 & N_i(\mathbf{x}_g^G) n_x \\ 0 & 0 & N_i(\mathbf{x}_g^G) n_y \end{pmatrix} l_g^C, \quad (57)$$

Finally, the smoothed element geometric stiffness matrix can be obtained as

$$\tilde{\mathbf{K}}_g = \int_{\Omega} \tilde{\mathbf{B}}_g^T \hat{\boldsymbol{\sigma}}_0 \tilde{\mathbf{B}}_g d\Omega = \sum_{C=1}^{nc} \tilde{\mathbf{B}}_{gC}^T \hat{\boldsymbol{\sigma}}_0 \tilde{\mathbf{B}}_{gC} A_C, \quad (58)$$

where  $nc$  is the number of smoothing cells, chosen to be 1 for evaluating the smoothed geometric stiffness matrix.

The analysis described above forms the basis of the four-node quadrilateral flat shell element, named MISQ24 (Mixed Interpolation Smoothing Quadrilateral element with 24 DOFs) which passed the patch tests and hence possesses proper convergence properties [27], for analysis of plate and shell structures.

#### 4. Numerical examples

In this section, a number of numerical examples are presented to demonstrate the performance of the MISQ24 element in buckling and free vibration analysis of various plate/shell panel structures. In all examples, the material properties are assumed to be the same in all the layers. The ply angle of each layer is measured from the global  $x$ -axis to the fibre direction. The thickness of each layer is identified. All the units of the model data are assumed to be consistent and therefore are not specified. Unless otherwise specified, shear correction factors  $k_1^2 = k_2^2 = \frac{\pi^2}{12}$  are used for all computations. The following two sets of typical graphite-epoxy material properties are used in the analysis:

- Material I:  $E_1/E_2 = 3, 10, 20, 30, 40$ ;  $G_{12} = G_{13} = 0.6E_2$ ;  $G_{23} = 0.5E_2$ ;  $\nu_{12} = \nu_{13} = \nu_{23} = 0.25$ ,  $\rho = 1$ .
- Material II:  $E_1/E_2 = 25$ ;  $G_{12} = G_{13} = 0.5E_2$ ;  $G_{23} = 0.2E_2$ ;  $\nu_{12} = \nu_{13} = \nu_{23} = 0.25$ ,  $\rho = 1$ .

##### 4.1. Laminated square plates under uniaxial compression

This section deals with the uniaxial buckling analysis of laminated square plates as shown in Figure 6 with different modulus ratios, span-to-thickness ratios, number of layers and mixed boundaries.

###### 4.1.1. Convergence study and effect of modulus ratios

A simply supported four-layer cross-ply  $[0^0/90^0/90^0/0^0]$  square laminated plate is chosen to study the convergence of the present method using MISQ24 element. The span-to-thickness ratio of the plate  $a/h$  is taken to be 10 in the computation.

Table 1 shows the convergence and comparison of the normalized fundamental frequencies of the present method with other solutions for various degrees of

orthotropy of the individual layers. It is found that the MISQ24 element yields accurate results in a wide range of  $E_1/E_2$  ratios.

The effect of various modulus ratios  $E_1/E_2$  on the accuracy of the critical buckling load is displayed in Figure 7. It can be seen that the present results are in good agreement with the 3D elasticity solutions [28] and slightly better than FSDT-based RPIM's solutions [29]. It is also observed that the present solution using MISQ24 element is quite insensitive to the variation of modulus ratios.

#### 4.1.2. Effect of span-to-thickness ratio

The effect of the span-to-thickness ratio ( $a/h$ ) on the uniaxial critical buckling load is studied for simply supported symmetric/antisymmetric 2-layer cross-ply  $[0^0/90^0]$  and angle-ply  $[-45^0/45^0]$  square plates made of Material I having  $E_1/E_2 = 40$ . The results obtained by the present MISQ24 element are shown in Table 2 and Table 3 in comparison with those obtained by FSDT and HSDT [30, 31, 32].

The numerical results show that the present solutions converge with mesh refinement for various span-to-thickness ratios  $a/h = 10, 20, 50, 100$ . It is observed that the critical buckling loads increase with increasing span-to-thickness ratio for both cross-ply and angle-ply laminates. The obtained numerical results are comparable with other solutions and in closer agreement with the HSDT than the FSDT results.

#### 4.1.3. Effect of mixed boundaries

The influence of the mixed boundary conditions and span-to-thickness ratio are now considered. The plate is always simply supported (S) along the edges parallel to the  $y$ -axis while the other edges have simply supported (S), clamped (C) or free (F) boundary conditions. The notation SSFC, for example, refers to the simply supported condition of the two edges parallel to the  $y$ -axis and the free and fully clamped conditions for the two edges parallel to the  $x$ -axis as shown in Figure 6. The 10-layer  $[0^0/90^0]_5$  square plate is analyzed with  $E_1 = 40E_2$  (Material I) and a  $10 \times 10$  mesh .

Table 4 contain the normalized critical buckling loads for various mixed boundaries obtained by the present method and other solutions using FSDT-based MLSQD method [33], RKPM's results by Wang et al. [34] and FSDT, HSDT solutions of Reddy and Khdeir [35]. It can be seen that the accuracy of the present method compares very well with FSDT solutions and other numerical results cited here.

The fundamental buckling mode of the 10-layer  $[0^0/90^0]_5$  plate under various edge conditions are shown in Figure 8.

#### 4.2. Laminated skew plates under uniaxial compression

This section deals with 4-layer symmetric cross-ply skew laminated plates under uniaxial compression as shown in Figure 9. Simply supported conditions at the four edges are considered with various skew angles from 0 to  $30^0$ . The span-to-thickness ratio  $a/h$  is taken to be 10, 20, 50 and 100 and the entire plate is modelled using  $10 \times 10$  mesh. In this problem, the material properties used for each individual layer are:  $E_1 = 128$  GPa,  $E_2 = 11$  GPa,  $G_{12} = G_{13} = 4.48$  GPa,  $G_{23} = 1.53$  GPa and  $\nu_{12} = \nu_{13} = \nu_{23} = 0.25$ .

Table 5 presents the normalized critical buckling load obtained by the present MISQ24 elements together with those of Chakrabarti and Sheikh [30] and Hu and Tzeng [36]. It can be seen that there is a good agreement between the present results and other existing solutions. Numerical results also show that the critical buckling load increases as the skew angle or as the span-to-thickness ratio increases.

#### 4.3. Laminated square plates under biaxial compression

In this section, 3-layer symmetric cross-ply  $[0^0/90^0/0^0]$  square plate is chosen to demonstrate the computation of the bi-axial buckling loads. The plate is of width  $a$  and thickness  $h$  and the span-to-thickness ratio  $a/h$  is taken to be 10. Material I is used in this computation.

Firstly, the effect of modulus ratio  $E_1/E_2$  on the critical bi-axial buckling load is studied. Table 6 reports the normalized critical buckling loads obtained by the present elements together with the FSDT solution of Fares and Zenkour [37] and HSDT solution of Khdeir and Librescu [38]. The present results in general indicate a good agreement with other referenced results and closer to those of HSDT than FSDT. It is also observed that the critical bi-axial buckling load increases with  $E_1/E_2$  ratios.

The effect of mixed edge support conditions on the critical biaxial buckling load is now investigated. Table 7 reports the present critical biaxial buckling loads together with the FSDT solutions in References [38, 39] and HSDT solutions in References [29, 38]. Once again, the MISQ24 element exhibits a good agreement with other numerical results cited here.

#### 4.4. Uniaxial buckling of multi-layer cylindrical shallow shell panels

This section deals with the uniaxial buckling analysis of simply supported cross-ply laminated cylindrical shell panels as shown in Figure 10 with different span-to-thickness ratios and number of layers.

##### 4.4.1. Effect of span-to-thickness ratio

A symmetric cross-ply 5-layer  $[0^0/90^0/0^0/90^0/0^0]$  shell panel is chosen for investigation. The panel is simply supported at all edges, with aspect ratio  $a/b = 1$  and  $R/a = 20$ . In this problem, the material properties used for each individual layer are:  $E_1/E_2 = 40$ ;  $G_{12} = G_{13} = 0.5E_2$ ;  $G_{23} = 0.6E_2$ ;  $\nu_{12} = \nu_{13} = \nu_{23} = 0.25$ .

Table 8 reports the normalized critical buckling loads obtained by MISQ24 element for various of span-to-thickness ratio  $a/h$  together with FSDT-based higher order element solutions [40, 41] and an analytic FSDT solution [42]. It can be seen that the MISQ24 element shows a slightly better performance than those of Kumar et al. [40], Prusty and Satsangi [41] for ratios  $a/h < 50$ . It is also observed that an increase of ratio  $a/h$  leads to higher critical buckling loads but this effect is minor with  $a/h > 50$ .

##### 4.4.2. Effect of the number of layers

The effect of the number of layers on the critical buckling load is now studied with  $a/h = 5$  and 10. A simply supported cross-ply  $k$ -layer  $[0^0/90^0/\dots]_k$  cylindrical shallow shell having Material II, with aspect ratio  $R/a = 2$  and  $a/b = 1$  is considered.

Table 9 reports the normalized critical buckling loads obtained by the present elements together with the analytic solution of [43] with various value of  $k$ . The numerical results show that the solutions obtained with the present MISQ24 elements are in good agreement with the analytic solution. The effect of the number of layers is also found to be a weak influence on the critical buckling loads.

#### 4.5. Free vibration of square laminated plates

This section deals with cross-ply laminated square plates with various span-to-thickness ratios, number of layers, boundary conditions and lay-up stacking sequences. The geometry data of the plate used in these analyses are shown in Figure 6.

##### 4.5.1. Mesh distortion

A simply supported 4-layer cross-ply  $[0^0/90^0/90^0/0^0]$  square plate is chosen to study the influence of mesh distortion. The distorted elements created by irregular

interior nodes which are derived from a set of regular nodes by using a controlling distortion factor  $s$  with the following expressions:

$$x' = x + r_c s \Delta x, \quad y' = y + r_c s \Delta y, \quad (59)$$

where  $r_c$  is a computer-generated random number between  $-1.0$  and  $1.0$ ,  $\Delta x, \Delta y$  are initial regular element sizes in the  $x$ - and  $y$ -directions, respectively and  $s \in [0, 0.4]$  is used to control the shapes of the distorted elements: the bigger value of  $s$ , the more irregular the shape of generated elements. A mesh of  $14 \times 14$  elements is chosen in this analysis and typical corresponding irregular meshes are shown in Figure 11.

The effect of mesh distortion on the fundamental frequency of the plate obtained by the present method is shown in Table 10 and Figure 12. It is found that the accuracy of the fundamental frequencies associated with irregular mesh decreases in comparison with regular meshes. However, the deterioration is very small and the overall performance is insensitive to mesh distortion as the maximum error of frequency is below 0.3% (in the case of  $E_1/E_2 = 10$ ).

#### 4.5.2. Effect of span-to-thickness ratio

This section deals with the effect of the span-to-thickness ratio ( $a/h$ ) on the fundamental frequency of a simply supported or clamped square cross-ply plate made of material having  $E_1/E_2 = 40$ . Table 11 presents a convergence study on the normalized fundamental frequency. The present numerical results are comparable with those of Reddy and Phan [31] who used higher-order shear deformation theory, Liew [44] who used a p-Ritz solution, Wu and Chen [45] who used local higher-order theory, Matsunaga [46] who used global higher-order theory, Striz *et al.* [47] who used higher-order individual-layer theory and Zhen and Wanji [48] who used global-local higher-order theory. However, it can be seen that the present results are in closer agreement with results of Liew than other results cited here. From Table 11, it is also noticed that the span-to-thickness ratio has a considerable effect on the fundamental frequency of plates at lower  $a/h$  ratios. At higher  $a/h$  ratios ( $a/h > 25$ ), the influence on the fundamental frequency is minor.

Table 12 reports the first four modes of a clamped unsymmetric cross-ply  $[0^0/90^0]$  square plate with different thickness ratios. It can be seen that the present method yields converged solution with mesh refinement and numerical results with a  $14 \times 14$  mesh are in good agreement with the 3D laminate solutions of Liew [49] for all values

of  $a/h$  ratio. It is also observed that the normalized frequencies increase with the increasing of  $a/h$ .

#### 4.5.3. Effect of mixed boundaries and span-to-thickness ratio

The influence of the mixed boundary conditions and span-to-thickness ratio is now considered. The plate is simply supported along the edges parallel to the  $y$ -axis while the other edges have simply supported (S), clamped (C) or free (F) boundary conditions. The three layer cross-ply  $[0^0/90^0/0^0]$  square plate is analyzed with  $E_1 = 40E_2$  and a  $14 \times 14$  mesh. Table 13 contains the normalized fundamental frequencies for various span-to-thickness ratios obtained by the present method together with the solution of Ferreira *et al.* [50] and exact solutions [17, 38]. It can be seen that the accuracy of the present method compares very well with exact solutions and other numerical results.

#### 4.6. Free vibration of skew laminated plates

This section deals with five-layer symmetric cross-ply and angle-ply skew laminated plates. Simply supported and clamped edges are considered with various skew angles  $\alpha$  from  $0^\circ$  to  $60^\circ$ . The span-to-thickness ratio  $a/h$  is taken to be 10 and the entire plate is modelled using  $6 \times 6$ ,  $10 \times 10$  and  $14 \times 14$  meshes. A representative sketch of the  $10 \times 10$  mesh used in the analysis is displayed in Figure 9.

Table 14 presents the normalized fundamental frequencies of the cross-ply skew plate  $[90^0/0^0/90^0/0^0/90^0]$  with simply supported and clamped edges while Table 15 shows the normalized fundamental frequencies of the angle-ply  $[45^0/-45^0/45^0/-45^0/45^0]$  plate with simply supported and clamped boundaries. The results calculated using MLSAQ method by Liew *et al.* [51] and B-spline Rayleigh-Ritz method of Wang *et al.* [52] are also listed for comparison. It can be seen that there is a good agreement between the present results and other existing solutions for both cases of cross-ply and angle-ply laminates. The numerical accuracy is slightly dependent on the skew angle  $\alpha$  (accuracy deteriorates with increasing  $\alpha$ ) but insensitive to lay-up sequence.

#### 4.7. Free vibration of circular laminated plates

A circular symmetric 4-layer  $[\theta/-\theta/-\theta/\theta]$  laminated plate with a diameter  $D$  and a thickness  $h$  as shown in Figure 13 is analysed. The span-to-thickness ratio  $a/h$  is taken to be 10 in the computation. Two types of boundary conditions,

simply supported (SSSS) and clamped (CCCC) with various fibre orientation angles  $\theta = 0^\circ, 15^\circ, 30^\circ, 45^\circ$  are considered.

The effect of the ply angle  $\theta$  on the normalized fundamental frequency of the simply supported and clamped circular laminated plate is presented in Table 16. The natural frequencies of the first six modes in the case of clamped edge conditions are presented in Table 17 while the corresponding mode shapes (in the case of  $\theta = 45^\circ$ ) are depicted in Figure 14. It is observed that the numerical results obtained by the present method are comparable with Liew's results [51].

#### 4.8. Free vibration of laminated cylindrical shell panel

The cross-ply laminated cylindrical panel with a radius  $R = 100$ , a side length  $L = 20$  and an angle  $\varphi = 0.1$  radian, subjected to simply supported boundaries is analysed. The total thickness of the panel is  $h = 0.2$ . All layers have equal thickness and are made of the same material:  $E_1/E_2 = 25$ ,  $G_{12} = G_{13} = 0.5E_2$ ,  $G_{23} = 0.2E_2$ ,  $\nu_{12} = \nu_{13} = \nu_{23} = 0.25$ ,  $\rho = 1$ . The SCFs are assumed to be  $5/6$ . Three kinds of lay-up sequence:  $[0^0/90^0]$ ,  $[0^0/90^0/0^0]$  and  $[0^0/90^0/90^0/0^0]$  are considered. Considering only doubly symmetric modes, a quadrant designated as ABCD as shown in Figure 15 is modeled. The  $4 \times 4$ ,  $6 \times 6$  and  $8 \times 8$  meshes are used in computing the fundamental frequencies associated with the doubly symmetric modes. The convergence study of the normalized fundamental frequency is presented in Table 18. The present results are also compared with other numerical solutions such as results of Liu and To using layer-wise (LW) shell element [53], of Jayasankar using 9-node degenerated shell element [54] and the analytical solution by Reddy [55].

It can be seen that the accuracy of the present element compare very favorably with other elements and the method is also convergent with mesh refinement. The present element can provide accurate prediction of the solution with much reduced degrees of freedom and its performance with respect to analytical solution is excellent.

#### 4.9. Free vibration of laminated spherical shell panel

A clamped nine-layered cross-ply  $[0^0/90^0/0^0/90^0/0^0/90^0/0^0/90^0/0^0]$  laminated spherical panel as shown in Figure 16 is considered. The panel has a radius  $R = 10$  and a side length  $a = 1$ . The total thickness of the panel is  $h = 0.01$ . All layers are of equal thickness and same material properties:  $E_1 = 2.0685 \times 10^{11}$ ,  $E_2 = E_1/40$ ,  $G_{12} = G_{13} = 0.5E_2$ ,  $G_{23} = 0.6E_2$ ,  $\nu_{12} = 0.25$  and  $\rho = 1605$ . The SCFs are

$k_1^2 = k_2^2 = 5/6$ . Three different finite element meshes are used ( $6 \times 6$ ,  $10 \times 10$ , and  $14 \times 14$ ) for modelling the whole panel.

Table 19 gives the first four normalized natural frequencies obtained by the present method in comparison with the solution of Jayasankar *et al.* [54] using nine-node degenerated shell element while Figure 17 depicts the corresponding mode shapes. It can be seen that the present results agree well with the solutions given by Jayasankar *et al.*

## 5. Conclusion

In this paper, the flat shell element MISQ24 [16] is further developed and successfully applied to analyse the buckling and free vibration analysis of laminated plate/shell structures within the framework of the FSDT. In contrast to general trend to use curved higher-order finite elements for analysis of shells, it is shown that the flat element formulation herein is adequately accurate and stable in all test cases. Several numerical investigations are conducted and the obtained results are in excellent agreement with those of other efficient numerical models and analytic solutions in the literature. The effect of various parameters on the critical buckling load and fundamental frequency is illustrated and discussed.

It is observed that the present element is relatively simple but yields good accuracy for many thin to moderately thick laminated plates/shells without shear locking or spurious modes. Since the integration is done on the element boundaries for the bending, membrane and geometric terms, the present element remains accurate even with badly-shaped elements while computational cost is reduced in comparison with other methods based on domain integrations.

## 6. Acknowledgements

The supports from the Computational Engineering & Science Research Center (CESRC) and the Centre of Excellence in Engineered Fibre Composites (CEEFC), University of Southern Queensland, Australia, are gratefully acknowledged. The authors would like to thank all reviewers for their helpful comments.

## References

- [1] H. T. Y. Yang, S. Saigal, A. Masud, R. K. Kapania, A survey of recent shell element, *International Journal for Numerical Methods in Engineering* 47 (1-3) (2000) 101–127.
- [2] A. W. Leissa, A review of laminated composite plate buckling, *Applied Mechanics Reviews* 40 (5) (1987) 575–591.
- [3] M. Aydogu, Comparison of Various Shear Deformation Theories for Bending, Buckling, and Vibration of Rectangular Symmetric Cross-ply Plate with Simply Support, *Journal of Composite materials* 40 (2006) 2143–2155.
- [4] S. Q. Mohamad, Recent research advances in the dynamic behavior of shell: 1989–2000, Part 1: Laminated composite shells, *ASME Applied Mechanics Reviews* 55 (4) (2002) 325–350.
- [5] K. M. Liew, K. C. Hung, M. K. Lim, Three-dimensional vibration of rectangular plates: Effects of thickness and edge constraints, *Journal of Sound and Vibration* 182 (5) (1995) 709–727.
- [6] K. M. Liew, T. M. Teo, Three-dimensional vibration analysis of rectangular plates based on differential quadrature method, *Journal of Sound and Vibration* 220 (4) (1999) 577–599.
- [7] K. M. Liew, T. M. Teo, J.-B. Han, A continuum three-dimensional vibration analysis of thick rectangular plates, *International Journal of Solids and Structures* 30 (24) (1993) 3357–3379.
- [8] K. M. Liew, K. C. Hung, M. K. Lim, Three-dimensional vibration of rectangular plates : Variance of simple support conditions and influence of in-plane inertia, *International Journal of Solids and Structures* 31 (23) (1994) 3233–3347.
- [9] K. M. Liew, T. M. Teo, J.-B. Han, Comparative accuracy of DQ and HDQ methods for three-dimensional vibration analysis of rectangular plates, *International Journal for Numerical Methods in Engineering* 45 (1999) 1831–1848.
- [10] E. Providas, M. A. Kattis, An assessment of two fundamental flat triangular shell elements with drilling rotations, *Computers and Structures* 77 (2000) 129–139.
- [11] C.-K. Choi, T.-Y. Lee, Efficient remedy for membrane locking of 4-node flat shell elements by non-conforming modes, *Computer Methods in Applied Mechanics and Engineering* 192 (2003) 1961–1971.

- [12] K. M. Liew, W. Karunasena, S. Kitipornchai, C. C. Chen, Vibration of unsymmetrically laminated thick quadrilateral plates, *Journal of the acoustical society of America* 105 (3) (1999) 1672–1681.
- [13] G. Pimpinelli, An assumed strain quadrilateral element with drilling degrees of freedom, *Finite Element in Analysis and Design* 41 (2004) 267–283.
- [14] K. D. Kim, G. R. Lomboy, G. Z. Voyiadjis, A 4-node assumed strain quasi-conforming shell element with 6 degrees of freedom, *International Journal for Numerical Methods in Engineering* 58 (2003) 2177–2200.
- [15] K. Darilmaz, N. Kumbasar, An 8-node assumed stress hybrid element for analysis of shell, *Computers and Structures* 84 (2006) 1990–2000.
- [16] H. Nguyen-Van, N. Mai-Duy, T. Tran-Cong, An improved quadrilateral flat element with drilling degrees of freedom for shell structural analysis, *CMES: Computer Modeling in Engineering & Sciences* 49 (2) (2009) 81–112.
- [17] J. N. Reddy, *Mechanics of laminated composite plates and shells-Theory and analysis*, CRC Press, 2004.
- [18] S. Valchoutsis, Shear correction factors for plates and shells, *International Journal for Numerical Methods in Engineering* 33 (1992) 1537–1552.
- [19] D. J. Allman, A compatible triangular element including vertex rotations for plane elasticity analysis, *Computers and Structures* 19 (1984) 1–8.
- [20] A. Ibrahimbegovic, R. L. Taylor, E. L. Wilson, A robust quadrilateral membrane finite element with drilling degrees of freedom, *International Journal for Numerical Methods in Engineering* 30 (1990) 445–457.
- [21] T. J. R. Hughes, F. Brezzi, On drilling degrees of freedom, *Computer Methods in Applied Mechanics and Engineering* 72 (1989) 105–121.
- [22] C. S. Long, S. Geyer, A. A. Groenwold, A numerical study of the effect of penalty parameters for membrane elements with independent rotation fields and penalized equilibrium, *Finite Element in Analysis and Design* 42 (2006) 757–765.
- [23] J. Liu, H. R. Riggs, A. Tessler, A four-node, shear-deformable shell element developed via explicit Kirchhoff constraints, *International Journal for Numerical Methods in Engineering* 49 (2000) 1065–1086.
- [24] K. J. Bathe, E. N. Dvorkin, A four node plate bending element based on Mindlin-Reissner plate theory and a mixed interpolation, *International Journal for Numerical Methods in Engineering* 21 (1985) 367–383.

- [25] R. L. Taylor, Finite element analysis of linear shell problems, in: J. White-man (Ed.), *Proceeding of the Mathematics in Finite Element and Applications*, Academic Press, New York, 1987.
- [26] O. C. Zienkiewicz, R. L. Taylor, *The Finite Element Method*, vol. 2: *Solid Mechanics*, Butterworth Heinemann-Oxford, 5th edn., 2000.
- [27] H. Nguyen-Van, Development and application of assumed strain smoothing finite element technique for composite plate/shell structures, Ph.D. thesis, University of Southern Queensland, 2009.
- [28] A. K. Noor, Stability of Multilayered Composite Plates, *Fibre Science and Technology* 8 (2) (1975) 81–89.
- [29] L. Liu, L. P. Chua, D. N. Ghista, Mesh-free radial basis function method for static, free vibration and buckling analysis of shear deformable composite laminates, *Composite Structures* 78 (2007) 58–69.
- [30] A. Chakrabarti, A. H. Sheikh, Buckling of Laminated Composite Plates by a New Element Based on Higher Order Shear Deformation Theory, *Mechanics of Composite Materials and Structures* 10 (4) (2003) 303–317.
- [31] J. N. Reddy, P. H. Phan, Stability and vibration of isotropic, orthotropic and laminated plates according to a higher order shear deformation theory, *Journal of Sound and Vibration* 89 (1985) 157–170.
- [32] N. D. Phan, J. N. Reddy, Analysis of laminated composite plates using a higher-order shear deformation theory, *International Journal for Numerical Methods in Engineering* 21 (1985) 2201–2219.
- [33] Y. Q. Huang, Q. S. Li, Bending and buckling analysis of antisymmetric laminates using the moving least square differential quadrature method, *Computer Methods in Applied Mechanics and Engineering* 193 (33–35) (2004) 3471–3492.
- [34] J. Wang, K. M. Liew, M. J. Tan, S. Rajendran, Analysis of rectangular laminated composite plates via FSDT meshless method, *International Journal of Mechanical Sciences* 44 (7) (2002) 1275–1293.
- [35] J. N. Reddy, A. A. Khdeir, Buckling and vibration of laminated composite plates using various plate theories, *AIAA Journal* 27 (12) (1989) 1808–1817.
- [36] H. T. Hu, W. L. Tzeng, Buckling analysis of skew laminate plates subjected to uniaxial inplane loads, *Thin-Walled Structures* 38 (2000) 53–77.

- [37] M. E. Fares, A. M. Zenkour, Buckling and free vibration of non-homogeneous composite cross-ply laminated plates with various plate theories, *Composite Structures* 44 (1999) 279–287.
- [38] A. A. Khdeir, L. Librescu, Analysis of symmetric cross-ply elastic plates using a higher-order theory. Part II: buckling and free vibration, *Composite Structures* 9 (1988) 259–277.
- [39] K. M. Liew, Y. Q. Huang, Bending and buckling of thick symmetric rectangular laminates using the moving least-squares differential quadrature method, *International Journal of Mechanical Sciences* 45 (1) (2003) 95–114.
- [40] L. R. Kumar, P. K. Datta, D. L. Prabhakara, Tension buckling and dynamic stability behaviour of laminated composite doubly curved panels subjected to partial edge loading, *Composite Structures* 60 (2003) 171–181.
- [41] B. G. Prusty, S. K. Satsangi, Finite element buckling analysis of laminated composite stiffened shells, *International Journal of Crashworthiness* 6 (2001) 471–484.
- [42] M. D. Sciuva, E. Carrera, Static buckling of moderately thick, anisotropic, laminated and sandwich cylindrical shell panels, *AIAA Journal* 28 (1990) 1782–1793.
- [43] H. Matsunaga, Vibration and stability of cross-ply laminated composite shallow shells subjected to in-plane stress, *Composite Structures* 78 (2007) 377–391.
- [44] K. M. Liew, Solving the vibration of thick symmetric laminates by Reissner/Mindlin plate theory and the p-Ritz method, *Journal of Sound and Vibration* 198 (1996) 343–360.
- [45] C. P. Wu, W. Y. Chen, Vibration and stability of laminated plates based on a local higher-order plate theory, *Journal of Sound and Vibration* 177 (1994) 503–520.
- [46] H. Matsunaga, Vibration and stability of cross-ply laminated composite plates according to a global higher-order plate theory, *Composite Structures* 145 (1991) 429–442.
- [47] A. G. Striz, K. N. Cho, C. W. Bert, Free vibration of laminated rectangular plates analyzed by higher-order individual-layer theory, *Journal of Sound and Vibration* 145 (1991) 429–442.
- [48] W. Zhen, C. Wanji, Free vibration of laminated composite and sandwich plates using global-local higher-order theory., *Journal of Sound and Vibration* 298 (2006) 333–349.

- [49] J. Z. Zhang, T. Y. Ng, K. M. Liew, Three-dimensional theory of elasticity for free vibration analysis of composite laminates via layerwise differential quadrature modelling, *International Journal for Numerical Methods in Engineering* 57 (2003) 1819–1844.
- [50] A. J. M. Ferreira, R. M. N. Jorge, C. M. C. Roque, Free vibration analysis of symmetric laminated composite plates by FSDT and radial basis functions, *Computer Methods in Applied Mechanics and Engineering* 194 (2005) 4265–4278.
- [51] K. M. Liew, Y. Q. Huang, J. N. Reddy, Vibration analysis of symmetrically laminated plates based on FSDT using the moving least squares differential quadrature method, *Computer Methods in Applied Mechanics and Engineering* 192 (2003) 2203–2222.
- [52] S. Wang, Free vibration analysis of skew fibre-reinforced composite laminates based on first-order shear deformation plate theory, *Computer & Structures* 63 (1997) 525–538.
- [53] M. L. Liu, C. W. S. To, Free vibration analysis of laminated composite shell structures using hybrid strain based layerwise finite elements, *Finite Elements in Analysis and Design* 40 (2003) 83–120.
- [54] S. Jayasankar, S. Mahesh, S. Narayanan, C. Padmanabhan, Dynamic analysis of layered composite shells using nine node degenerate shell elements, *Journal of Sound and Vibration* 299 (2007) 1–11.
- [55] J. N. Reddy, Exact solutions of moderately thick laminated shells, *ASCE Journal of Engineering Mechanics* 110 (1984) 794–809.

Table 1: Simply supported cross-ply  $[0^0/90^0/90^0/0^0]$  square plate: Convergence of normalized critical buckling loads with various  $E_1/E_2$  ratios and comparison with other solutions ( $\lambda^* = N_x a^2 / (E_2 h^3)$ ,  $a/h = 10$ )

Model	$E_1/E_2$					
	3	10	20	30	40	
MISQ24 (6×6)	5.583	10.279	15.803	20.308	24.080	
	(10×10)	5.409	9.978	15.360	19.759	23.446
	(12×12)	5.380	9.927	15.287	19.667	23.340
	(16×16)	5.352	9.878	15.214	19.577	23.236
		(1.096%)	(1.188%)	(1.298%)	(1.414%)	(1.551%)
(20×20)	5.321	9.809	15.064	19.339	22.912	
	(0.510%)	(0.481%)	(0.299%)	(0.181%)	(0.135%)	
FSDT-based RPIM [29]	5.401	9.985	15.374	19.537	23.154	
	(2.021%)	(2.284%)	(2.364%)	(1.207%)	(1.193%)	
HSDT [32]	5.114	9.774	15.298	19.957	23.340	
	(-3.400%)	(1.230%)	(1.858%)	(3.383%)	(2.006%)	
HSDT [38]	5.442	10.026	15.418	19.813	23.489	
	(2.796%)	(2.704%)	(2.657%)	(2.637%)	(2.657%)	
3D Elasticity [28]	5.294	9.762	15.019	19.304	22.881	

Values in parentheses correspond to relative error compared to 3D elasticity solution.

Table 2: Simply supported cross-ply  $[0^0/90^0]$  square plate with various  $a/h$  ratios: Convergence of normalized critical buckling loads and comparison with other solutions ( $E_1/E_2 = 40$ ,  $\lambda^* = N_x a^2 / (E_2 h^3)$ ).

Model		$a/h$			
		10	20	50	100
MISQ24	6×6	12.083	13.373	13.819	13.911
	10×10	11.604	12.798	13.210	13.296
	16×16	11.446	12.609	13.011	13.095
	20×20	11.360	12.551	12.906	13.039
FSDT [30]		11.349	12.510	12.879	12.934
FSDT [31]		11.353	12.515	12.884	12.939
HSDT [31]		11.563	12.577	12.895	12.942

Table 3: Simply supported angle-ply  $[45^0/-45^0]$  square plate with various  $a/h$  ratios: Convergence of normalized critical buckling loads and comparison with other solutions ( $E_1/E_2 = 25$ ,  $\lambda^* = N_x a^2/(E_2 h^3)$ ).

Model		$a/h$			
		10	20	50	100
MISQ24	$6 \times 6$	12.615	15.256	16.222	16.370
	$10 \times 10$	12.206	14.709	15.618	15.758
	$16 \times 16$	12.072	14.528	15.419	15.557
	$20 \times 20$	12.042	14.500	15.374	15.510
HSDT [30]		12.600	14.629	15.329	15.435
HSDT [32]		12.622	14.644	15.336	15.441

Table 4: Cross-ply 10-layer  $[0^0/90^0]_5$  square plate with various mixed boundaries: Comparison of normalized critical buckling loads with other solutions ( $E_1/E_2 = 40$ ,  $a/h = 10$ ,  $\lambda^* = N_x a^2/(E_2 h^3)$ ).

Model	SSSS	SSFF	SSCC	SSSC	SSFC	SSFS
MISQ24	25.534	12.131	34.531	32.874	14.356	12.543
MLSDQ [33]	25.338	12.030	34.604	–	–	–
RKPM [34]	25.703	12.224	35.162	32.950	14.495	12.658
FSDT [35]	25.450	12.092	34.837	32.614	14.358	12.524
HSDT [35]	25.423	12.077	35.376	32.885	14.351	12.506

Table 5: Simply supported cross-ply  $[90^0/0^0/0^0/90^0]$  skew plate with various skew angles and span-to-thickness ratios: Comparison of the critical buckling loads with other solutions ( $\lambda^* = N_x a^2/(E_2 h^3)$ ).

Skew Angle	Model	$a/h$			
		10	20	50	100
0	MISQ24	8.623	10.976	11.939	12.094
	HSDT [30]	9.392	11.324	12.029	12.138
	Hu and Tzeng [36]	–	–	–	12.045
10	MISQ24	8.979	11.600	12.757	12.960
	HSDT [30]	9.871	12.057	12.888	13.020
	Hu and Tzeng [36]	–	–	–	13.000
20	MISQ24	10.104	13.577	15.369	15.753
	HSDT [30]	11.367	14.441	16.701	15.915
	Hu and Tzeng [36]	–	–	–	15.636
30	MISQ24	12.185	17.314	20.294	21.050
	HSDT [30]	13.753	18.920	20.188	21.605
	Hu and Tzeng [36]	–	–	–	21.500

Table 6: Simply supported cross-ply  $[0^0/90^0/0^0]$  square plate with various modulus ratio: Comparison of the critical bi-axial buckling loads with other solutions ( $\lambda^* = N_x a^2 / (E_2 h^3)$ ).

Model	$E_1/\bar{E}_2$			
	10	20	30	40
MISQ24 ( $10 \times 10$ )	4.939	7.488	9.016	10.252
FSDT [37]	4.963	7.588	8.575	10.202
HSDT [38]	4.963	5.516	9.056	10.259

Table 7: Cross-ply  $[0^0/90^0/0^0]$  square plate with mixed boundaries: Comparison of normalized critical bi-axial buckling loads with other solutions ( $E_1/E_2 = 40$ ,  $a/h = 10$ ,  $\lambda^* = N_x a^2 / (E_2 h^3)$ ).

Model	SSSS	SSFF	SSCC	SSSC	SSFC
MISQ24 ( $10 \times 10$ )	10.252	1.858	13.249	11.613	5.964
MLSDQ [39]	10.120	1.926	13.225	11.523	5.517
RPIM [29]	10.091	1.928	12.952	–	–
FSDT [38]	10.202	1.937	13.290	11.602	5.551
HSDT [38]	10.259	1.937	13.288	–	–

Table 8: Simply supported cross-ply  $[0^0/90^0/0^0/90^0//0^0]$  cylindrical shell panel: Comparison of the normalized critical buckling loads with other solutions ( $\lambda^* = N_x a^2 / (E_2 h^3)$ ).

Model	$a/h$				
	10	20	30	50	100
MISQ24 ( $8 \times 8$ )	24.412	32.557	34.796	36.081	36.656
( $12 \times 12$ )	24.088	32.077	34.268	35.525	36.087
( $16 \times 16$ )	23.976	31.911	34.086	35.334	35.891
Kumar et al. [40]	23.97	31.79	–	35.40	36.85
Prusty and Satsangi [41]	23.96	31.89	33.98	35.39	36.84
FSDT [42]	24.19	31.91	34.04	35.42	36.86

Table 9: Simply supported cross-ply  $k$ -layer  $[0^0/90^0/...]_k$  cylindrical shallow shell: Comparison of normalized critical buckling loads ( $\lambda^* = N_x / (E_2 h)$ ,  $R/a = 2$ ,  $a/b = 1$ ).

$k$	$a/h = 5$		$a/h = 10$	
	MISQ24	Matsunaga [43]	MISQ24	Matsunaga [43]
2	0.2344	0.2227	0.0956	0.0879
3	0.2964	0.2660	0.1498	0.1424
4	0.2828	0.2763	0.1506	0.1400
5	0.3093	0.2973	0.1601	0.1561
10	0.2858	0.3487	0.1639	0.1686

Stacking sequence:  $k=2$ :  $[0^0/90^0]$ ;  $k=3$ :  $[0^0/90^0/0^0]$ .

Table 10: Simply supported cross-ply  $[0^0/90^0/90^0/0^0]$  square plate: Effect of mesh distortion on the normalized fundamental frequencies ( $\omega^* = (\omega a^2/h)\sqrt{\rho/E_2}$ ,  $a/h = 5$ ).

$E_1/E_2$	$s = 0$	$s = 0.1$	$s = 0.2$	$s = 0.3$	$s = 0.4$
40	10.8471	10.8476	10.8495	10.8528	10.8597
30	10.3224	10.3239	10.3257	10.3283	10.3354
20	9.5698	9.5712	9.5728	9.5749	9.5820
10	8.3094	8.3108	8.3125	8.3140	8.3207

Table 11: Simply supported cross-ply  $[0^0/90^0/90^0/0^0]$  square plate with various  $a/h$  ratios: Convergence of normalized fundamental frequencies and comparison with other solutions ( $\omega^* = (\omega a^2/h)\sqrt{\rho/E_2}$ ,  $E_1/E_2 = 40$ ).

Model		$a/h$					
		5	10	20	25	50	100
MISQ24	$6 \times 6$	11.0001	15.4187	18.0504	18.4839	19.1221	19.2939
	$10 \times 10$	10.8792	15.2201	17.7903	18.2122	18.8325	18.9992
	$14 \times 14$	10.8461	15.1658	17.7192	18.1380	18.7535	18.9189
p-Ritz [44]		10.8550	15.1434	17.6583	18.0718	18.6734	18.8359
Reddy & Phan [31]		10.9891	15.2689	17.6669	18.0490	18.4624	18.7561
Cho <i>et al.</i> [47]		10.673	15.066	17.535	18.054	18.670	18.835
Local theory [45]		10.682	15.069	17.636	18.055	18.670	18.835
Global theory [46]		10.6876	15.0721	17.6369	18.0557	18.6702	18.8352
Global-local theory [48]		10.7294	15.1658	17.8035	18.2404	18.9022	19.1566

Table 12: Clamped cross-ply  $[0^0/90^0]$  square plate with different thickness ratios: Convergence of fundamental frequencies and comparison with other solutions ( $\omega^* = (\omega a^2 h/\sqrt{\rho/E_2})$ ,  $E_1/E_2 = 40$ ).

$a/h$	Model	Mesh	Mode sequences			
			I	II	III	IV
5	MISQ24	$6 \times 6$	10.620	18.410	22.596	26.112
		$10 \times 10$	10.467	17.875	21.835	25.433
		$14 \times 14$	10.426	16.871	21.602	24.488
	3D layerwise [49]		10.559	16.998	21.908	25.296
10	MISQ24	$6 \times 6$	16.175	29.417	38.901	44.479
		$10 \times 10$	15.876	28.425	37.855	43.516
		$14 \times 14$	15.795	27.854	36.103	42.689
	3D layerwise [49]		15.559	27.089	35.468	42.216

Table 13: Cross-ply  $[0^0/90^0/0^0]$  square plate with various mixed boundaries and span-to-thickness ratios: Comparison of normalized fundamental frequencies with other solutions ( $\omega^* = (\omega a^2/h)\sqrt{\rho/E_2}$ ,  $E_1/E_2 = 40$ ).

$a/h$	Model	SSSS	SSSC	SSCC	SSFF	SSFS	SSFC
5	MISQ24	10.2780 (-0.117%)	10.6280 (-0.169%)	11.2387 (-0.242%)	4.0717 (0.461%)	4.5613 (0.381%)	5.9370 (0%)
	RBF [50]	10.307 (0.165%)	10.658 (0.113%)	11.274 (0.071%)	-	-	-
	Exact[38, 17]	10.290	10.646	11.266	4.053	4.544	5.937
10	MISQ24	14.7823 (0.110%)	17.1806 (0.033%)	19.6614 (-0.039%)	4.3679 (0.573%)	4.9401 (0.531%)	7.3372 (0.084%)
	RBF [50]	14.804 (0.257%)	17.199 (0.139%)	19.678 (0.046%)	-	-	-
	Exact[38, 17]	14.766	17.175	19.669	4.343	4.914	7.331
100	MISQ24	18.9095 (0.098%)	28.4750 (-0.091%)	40.5937 (-0.366%)	4.4835 (0.594%)	5.1007 (0.487%)	8.2665 (-0.030%)
	RBF [50]	18.355 (-2.837%)	28.165 (-1.179%)	40.234 (-1.249%)	-	-	-
	Exact[38, 17]	18.891	28.501	40.743	4.457	5.076	8.269

Values in parentheses correspond to relative error compared to exact solution.

Table 14: Cross-ply  $[90^0/0^0/90^0/0^0/90^0]$  skew plate with various skew angles: Convergence of fundamental frequencies and comparison with other solutions ( $\omega^* = (\omega a^2\sqrt{\rho/E_2})/(\pi^2 h)$ ,  $E_1/E_2 = 40$ ,  $a/h = 10$ ).

BC	Model	Mesh	$\alpha$				$60^0$
			$0^0$	$15^0$	$30^0$	$45^0$	
SSSS	MISQ24	$6 \times 6$	1.6030	1.7267	2.1441	3.0021	4.7710
		$10 \times 10$	1.5797	1.6977	2.0963	2.9141	4.6033
		$14 \times 14$	1.5733	1.6896	2.0820	2.8855	4.5412
	MLSDQ [51]		1.5709	1.6886	2.1026	2.8798	4.4998
	B-spline[52]		1.5699	-	2.0844	2.8825	-
CCCC	MISQ24	$6 \times 6$	2.4550	2.5528	2.8901	3.6260	5.2538
		$10 \times 10$	2.4014	2.4958	2.8194	3.5200	5.0610
		$14 \times 14$	2.3869	2.4803	2.7998	3.4893	4.9989
	MLSDQ [51]		2.3790	2.4725	2.7927	3.4723	4.9430
	B-spline[52]		2.3820	-	2.7921	3.4738	-

Table 15: Angle-ply  $[45^0/-45^0/45^0/-45^0/45^0]$  skew plate with various skew angles: Convergence of fundamental frequencies and comparison with other solutions ( $\omega^* = (\omega a^2 \sqrt{\rho/E_2})/(\pi^2 h)$ ,  $E_1/E_2 = 40$ ,  $a/h = 10$ ).

B.C.	Model	Mesh	$\alpha$				
			$0^0$	$15^0$	$30^0$	$45^0$	$60^0$
SSSS	MISQ24	$6 \times 6$	1.8768	1.9255	2.1546	2.7185	4.1758
		$10 \times 10$	1.8491	1.8969	2.1093	2.6286	4.0249
		$14 \times 14$	1.8413	1.8889	2.0955	2.5672	3.9718
	MLSDQ [51]		1.8248	1.8838	2.0074	2.5028	4.0227
	B-spline[52]		1.8792	–	2.0002	2.4788	–
CCCC	MISQ24	$6 \times 6$	2.3551	2.4242	2.7566	3.5013	5.1549
		$10 \times 10$	2.3045	2.3713	2.6892	3.3977	4.9605
		$14 \times 14$	2.2908	2.3570	2.6708	3.3683	4.8982
	MLSDQ [51]		2.2787	2.3504	2.6636	3.3594	4.8566
	B-spline[52]		2.2857	–	2.6626	3.3523	–

Table 16: Circular 4-layer  $[\theta/-\theta/-\theta/\theta]$  laminated plates with various boundary conditions and ply angles: Comparison of fundamental frequencies with other solutions ( $\omega^* = (\omega a^2/h)\sqrt{\rho/E_2}$ ,  $E_1/E_2 = 40$ ,  $a/h = 10$ ).

Model	B.C	$\theta$			
		0	15	30	45
MISQ24	SSSS	16.168	16.448	16.924	17.162
MLSDQ [51]		16.167	16.475	16.928	17.119
MISQ24	CCCC	22.123	22.698	24.046	24.766
MLSDQ [51]		22.211	22.774	24.071	24.752

Table 17: Clamped circular 4-layer  $[\theta/-\theta/-\theta/\theta]$  laminated plate: Comparison of the normalized natural frequencies of the first six modes ( $\omega^* = (\omega a^2/h)\sqrt{\rho/E_2}$ ,  $E_1/E_2 = 40$ ,  $a/h = 10$ ).

$\theta$	Model	Mode					
		1	2	3	4	5	6
0	MISQ24	22.123	29.768	41.726	42.805	50.756	56.950
	MLSDQ [51]	22.211	29.651	41.101	42.635	50.309	54.553
15	MISQ24	22.698	31.568	43.635	44.318	53.468	60.012
	MLSDQ [51]	22.774	31.455	43.350	43.469	52.872	57.386
30	MISQ24	24.046	36.399	44.189	52.028	57.478	67.099
	MLSDQ [51]	24.071	36.153	43.968	51.074	56.315	66.220
45	MISQ24	24.766	39.441	43.817	57.907	57.945	66.297
	MLSDQ [51]	24.752	39.181	43.607	56.759	56.967	65.571

Table 18: Simply supported cross-ply cylindrical shell panel: Convergence of normalized fundamental frequencies  $\omega^* = (\omega L^2/h)\sqrt{\rho/E_2}$  for doubly symmetric modes and comparison with other solutions.

Model	Mesh	Lay-up		
		$[0^0/90^0]$	$[0^0/90^0/0^0]$	$[0^0/90^0/90^0/0^0]$
MISQ24	$4 \times 4$	17.099	20.585	20.703
	$6 \times 6$	16.873	20.367	20.481
	$8 \times 8$	16.794 (0.756%)	20.292 (-0.197%)	20.404 (0.211%)
LW theory [53]	$8 \times 8$	17.390 (4.332%)	20.960 (3.089%)	20.960 (2.942%)
9-node element [54]	$5 \times 5$	17.7 (6.192%)	-	-
		16.668	20.332	20.361

Note that values in parentheses is relative errors with respect to analytic solutions

Table 19: Clamped 9-layer  $[(0^0/90^0)_4/0^0]$  cross-ply spherical shell panel: Comparison of the normalized frequencies  $\omega^* = (\omega a^2/h)\sqrt{\rho/E_2}$  with other solutions.

Model	Mesh	Mode 1	Mode 2	Mode 3	Mode 4
MISQ24	$6 \times 6$	69.61	98.25	118.15	136.05
	$10 \times 10$	67.94	88.24	104.45	119.73
	$14 \times 14$	67.51	86.00	101.27	115.88
9-node element [54]	$15 \times 15$	67.43	84.16	99.71	113.70

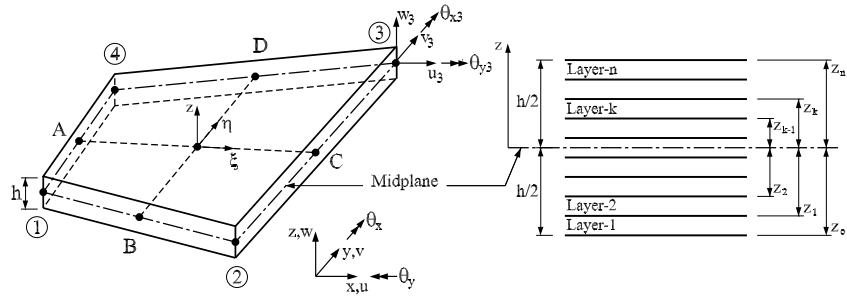


Figure 1: A quadrilateral laminated plate element consisting of  $n$  layers.

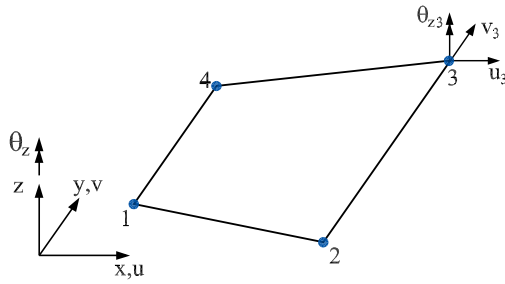


Figure 2: A 4-node quadrilateral element with drilling degrees of freedom

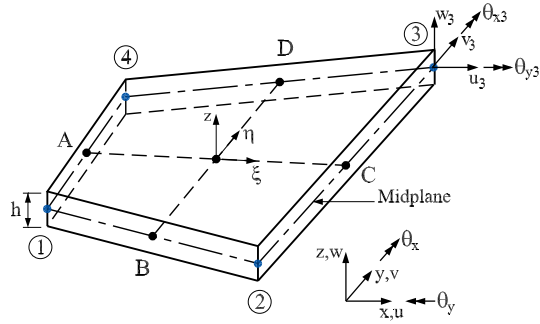


Figure 3: A 4-node quadrilateral plate bending element

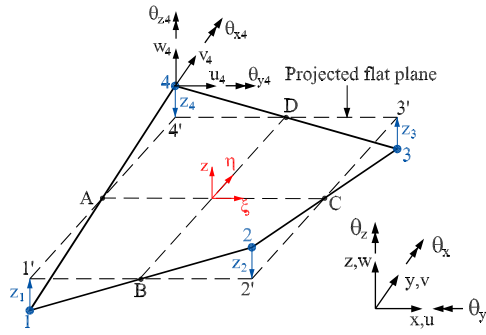


Figure 4: The projection of a warped shell element into a flat mean plane

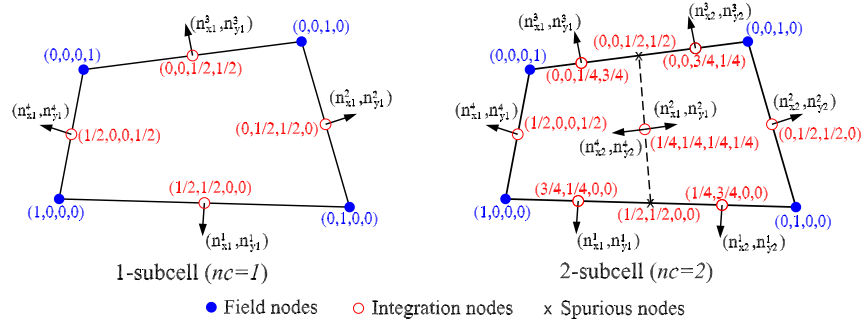


Figure 5: Subdivision of an element into  $nc$  smoothing cells and the values of shape functions at nodes.

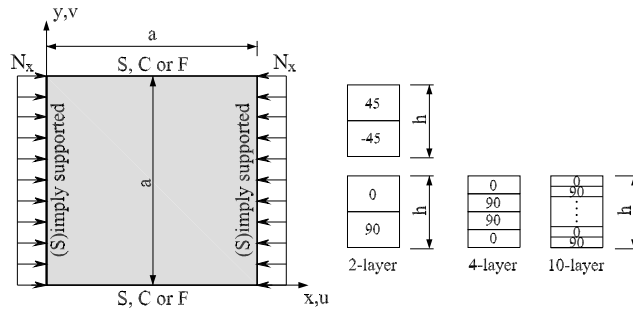


Figure 6: Cross-ply square laminated plate subjected to in-plane compression.

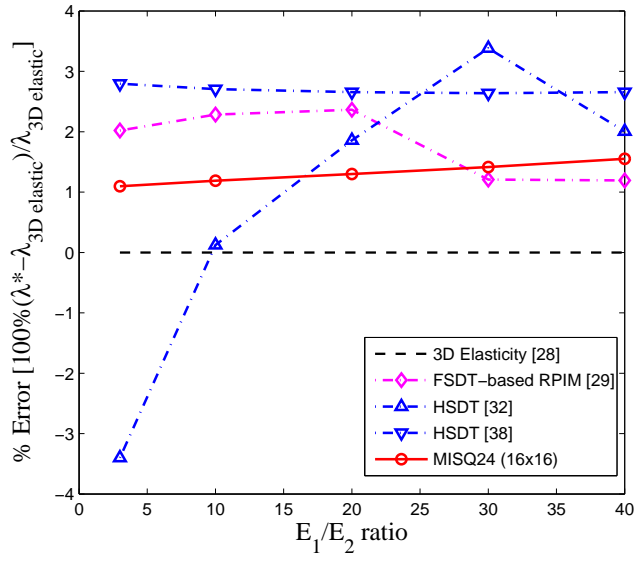


Figure 7: Effect of modulus ratios on the accuracy of critical buckling loads

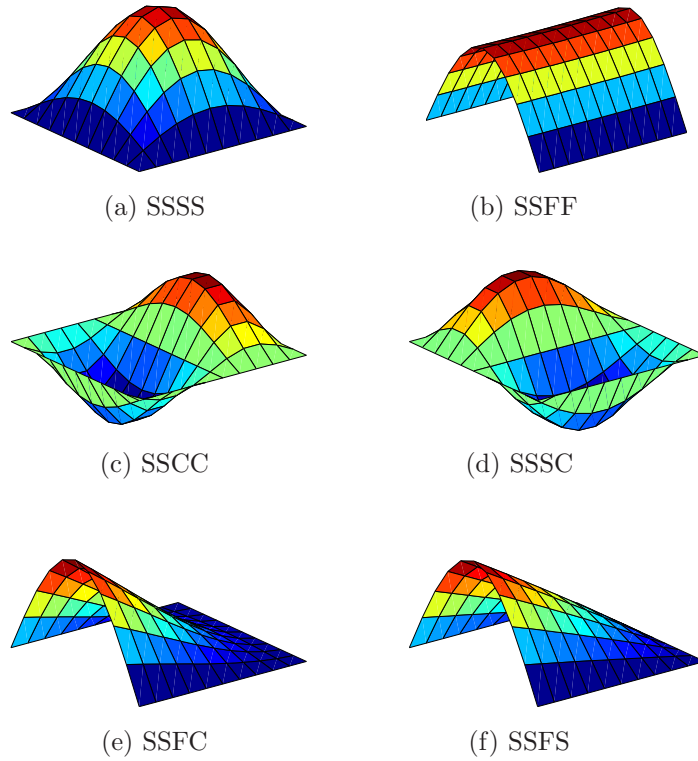


Figure 8: Fundamental buckling mode of cross-ply 10-layer  $[0^0/90^0]_5$  square plate with various mixed boundaries.

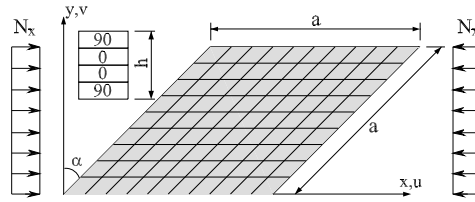


Figure 9: Geometry and discretization of cross-ply skew plates

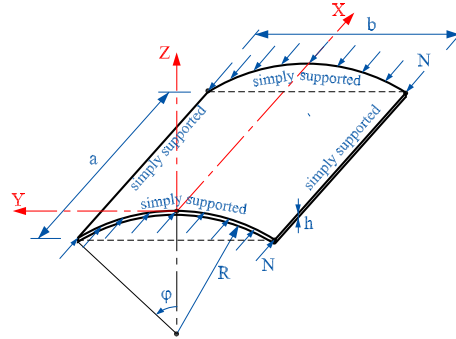


Figure 10: Geometry data of a cylindrical shallow shell subjected to uniaxial compression.

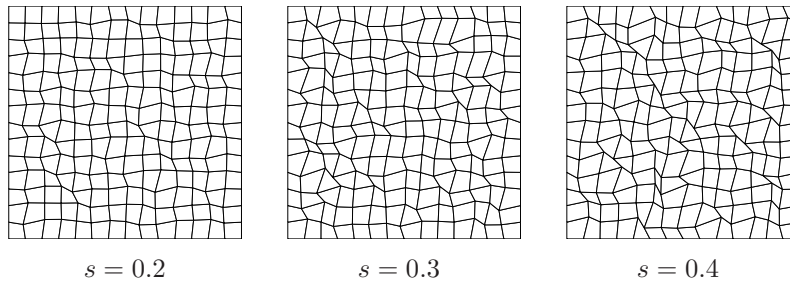


Figure 11: Typical irregular meshes with various distortion factor  $s$ .

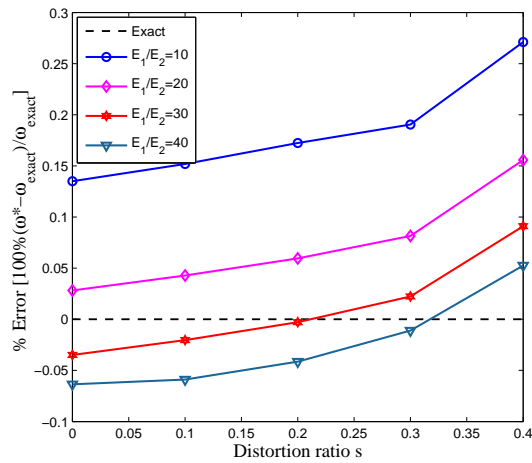


Figure 12: Square cross-ply  $[0/90/90/0]$  laminated plate: Effect of mesh distortion on the accuracy of the fundamental frequency.

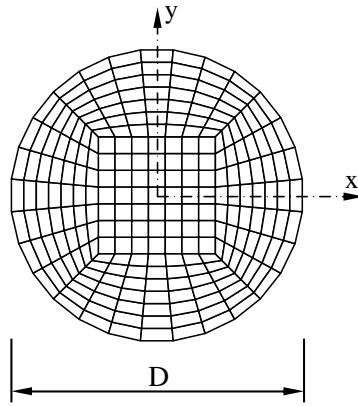


Figure 13: Geometry and discretization of a circular laminated plate

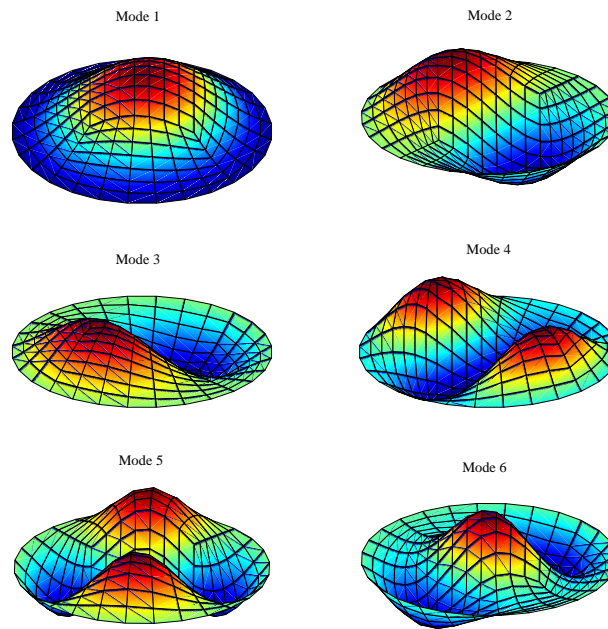


Figure 14: Clamped circular angle-ply  $[45^0 / -45^0 / -45^0 / 45^0]$  laminated plate: the first six mode shapes.

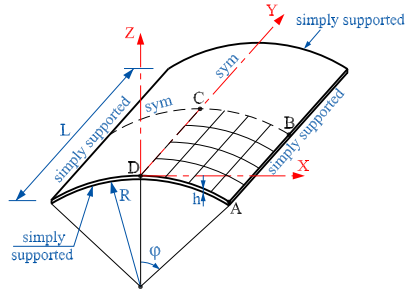


Figure 15: Geometry and discretization of a laminated cylindrical shell panel.

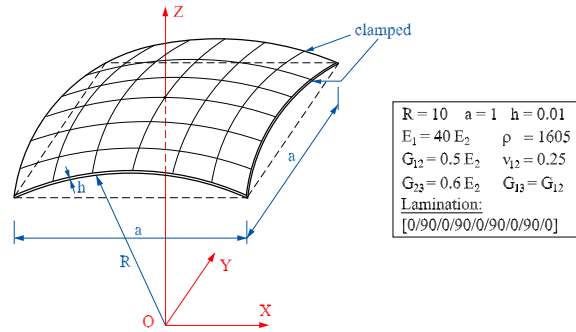


Figure 16: Geometry and discretization of a laminated spherical shell panel.

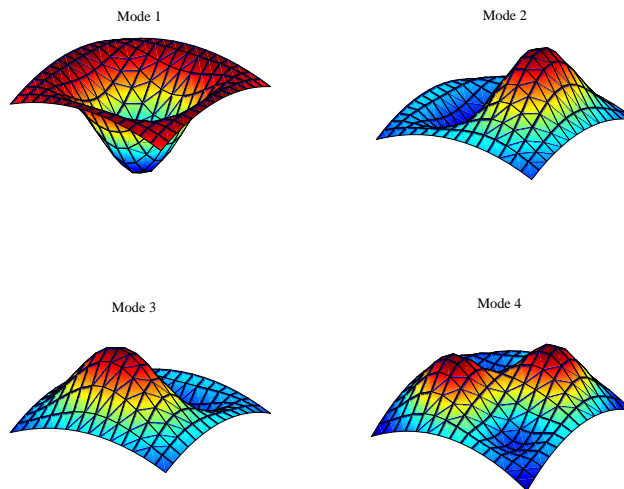


Figure 17: Clamped 9-layer cross-ply  $[(0^0/90^0)_4/0^0]$  spherical shell: the first four mode shapes.